Multifractality in aeroelastic response as a precursor to flutter

J. Venkatramani [a] Vineeth Nair [b] R.I. Sujith [b] Sayan Gupta [a] Sunetra Sarkar [b,*]

[a] *Department of Applied Mechanics, Indian Institute of Technology Madras, Chennai 600036 India*

[b] *Department of Aerospace Engineering, Indian Institute of Technology Madras, Chennai 600036, India*

Abstract

Wind tunnel tests on a NACA 0012 airfoil has been carried out to study the transition in aeroelastic response from an initial state characterised by low-amplitude aperiodic fluctuations to aeroelastic flutter when the system exhibits limit cycle oscillations. An analysis of the aeroelastic measurements reveals multifractal characteristics in the pre-flutter regime. This has not been studied in the literature. As the flow velocity approaches the flutter velocity from below, a gradual loss in multifractality is observed. Measures based on the generalised Hurst exponents are developed and are shown to be effective precursors to warn against impending aeroelastic flutter. The results in this study would be useful for health monitoring in aeroelastic structures.

Key words: Aeroelastic flutter, Multifractals, Hurst exponent, Wind tunnel experiments, Precursor, Structural health monitoring

1 Introduction

The dynamical behaviour of slender flexible structures in flows can be phenomenologically very rich due to the mutual interaction effects where the forces exerted by the fluid in the structure become dependent on the dynamics of the structure. In certain flow regimes, the coupling between the forces exerted by the fluid and the structure result in zero damping in the combined fluid-structure system leading to self-sustained oscillations termed as aeroelastic flutter. In the parlance of nonlinear dynamics, these oscillations represent limit cycle oscillations (LCO) which appear when the flow velocity exceeds a critical value - termed as the flutter velocity. As the flow velocity is increased further, the amplitude of the response

* Corresponding author: sunetra@iitm.ac.in, Phone: +91 44 2257 4024, FAX: +91 44 2257 4002

oscillations increase. At flow velocities below the flutter velocity, the structural damping dominates leading to the structure oscillations to eventually die down. The flutter velocity represents a Hopf bifurcation point [1].

Aero-elastic flutter is an undesirable phenomenon as the sustained oscillations post flutter could lead to structural damage due to fatigue in metals and debonding or delamination in composites - either of which eventually leads to structural degradation and failure. From the perspective of health monitoring of aeroelastic structures, it is important to ensure the operating conditions of the structure lie within the stable regime characterised by the pre-flutter domain. Identification of the stability boundaries for such aeroelastic structures therefore constitute a very important step in design and health monitoring. This has led to studies being devoted in the literature on methods for analyzing the stability boundaries of such fluid-structure interaction problems. Analytical studies carried out in the literature are based on developing suitable mathematical models for the slender structure and the forces that arise due to the presence of the flow [2, 3, 4, 5, 6, 7]. Here, the challenges lie in modelling the nonlinearities in the stiffness and damping properties of the structure [8, 9] and developing expressions that approximate the fluid forces that act on the structure.

Alternative methods for identification of the stability boundaries are based on analysis of the time histories of the aeroleastic response. For example, methods based on monitoring the damping levels in fluid-structure interaction system [6, 10],has been one of the early-methods used to estimate flutter boundary. However, this method becomes unsuitable in the presence of nonlinearity. An alternative methodology for identification of flutter boundary is the Zimmermann-Weissenburger Methodology (ZWM)[11]. This methodology derives a flutter margin based on Routh's stability criterion and was applied to a two degree of freedom system with quasi-steady aerodynamics. Subsequently, the ZWM was applied to systems with higher degrees of freedom as well [12]. Using an analytical model, an online flutter prediction tool called flutterometer was developed [13]. For the sake of modelling errors and uncertainties, parts of the model were updated through a nonlinear iterative algorithm that generates a "worst case flutter boundary". Despite the technique being robust, the proposed stability margins were found to be conservative [14]. In order to predict nonlinear aeroelastic behaviors like LCO, an expert system (ES) was developed [15] and tested on short duration transient data acquired from both experiments and numerics. It was observed that ES could successfully predict behaviors like LCO's, diverging oscillations etc. However, these methods were developed in the presence of freeplay nonlinearity in pitch degree of freedom and is suggested that the effectiveness of the ES depends upon an acurate estimation of the freeplay parameters. Further, the suitablity of this technique in the presence of other types of nonlinearities and wind gusts has not been explored.

Indeed, most studies on aeroelastic stability analysis were carried out under the assumptions of steady uniform flow. However, in real life conditions, the flow is seldom steady and are usually accompanied by fluctuations. These fluctuations could be either due to gust effects in the flows or due to turbulence, generated by the local flow conditions around the structure. The effect of fluctuations on the flow have significant influence on the structure response. For example, even in pre-flutter regimes, it has been shown that an impulsive gust loading in the flow can lead to transient growth in the structure response due to the transition of the system to higher stable branches in sub-critical bifurcating regimes [16]. Additionally, it has been observed that the dynamical system experiences sporadic bursts of oscillations prior to the setting of LCOs in the presence of fluctuating flows. These oscillations - termed as intermittent oscillations - have been reported in [17, 18, 19, 20, 21], but have not been investigated in details. In a recent study [22], similar intermittent oscillations in airfoils have been observed in wind tunnel experiments. Detailed experimental studies carried out revealed that the sporadic bursts of oscillations that began to appear at pre-flutter flow speeds become more frequent and of longer durations as the flow speed approached the flutter velocity. The repeating patterns of these intermittent oscillations were visualised using recurrence plots and precursors were developed that enabled predicting the onset of flutter. It must be remarked here that the existing studies in the literature on methods for identifying the stability boundaries of an aeroelastic system could identify the instability regimes only after the system has already lost stability, and therefore are not precursors in the strict sense.

Development of precursors to instability in dynamical systems - that range from engineering applications to geophysical systems as well as biological processes - have been studied extensively in the literature. Approaches that involve analyzing the response of dynamical systems in the frequency domain to estimate precursors have been carried out in [23, 24]. The bandwidth of the dominant frequency of the filtered response of a dynamical system subjected to broad band noise was used as a measure of the instability in [23]. A similar approach was used in [24] where the width of the hysteresis zone obtained from the filtered response of a nonlinear geophysical system was used as a measure to quantify the instability. However, exciting the dynamical system with an external stochastic excitation can qualitatively change the dynamics of the system and may not lead to accurate precursors; this has been demonstrated with reference to an acoustic system in [25] and highlights the drawback of these frequency domain approaches.

The focus of this paper is to investigate the small aperiodic oscillations that appear in the response of a NACA 0012 airfoil when subjected to flows in a low speed wind tunnel and to study the transition in the response dynamics from low amplitude aperiodic fluctuations to flutter as the mean flow speed is gradually increased. It is shown that the time histories of the response possess multifractal characteristics and displays scale invariance at flow speeds much lower than the flutter velocity. As the flow speed approaches the flutter velocity from below, the multifractality in the airfoil response gradually diminishes and eventually disappears with the onset of LCO. Measures that are based on quantifying the multifractality of time histories are developed that serve as precursors to forewarn impending flutter.

This paper is organized as follows. A brief description on fractals and multifractality in time histories, and measures of quantifying the multifractality is presented in Section 2. Section 3 provides details of the wind tunnel experiments and the set-up. Investigations on the multifractality of the measured response are discussed in details in Section 4. Section 5 details the development of suitable measures that serve as precursors to flutter. The salient features of this study are summarized in section 6. For the sake of completion, an appendix is provided which gives a brief description of the algorithm used for quantifying the multifractality in the measured time histories.

2 Multifractality

Fractal sets, which could represent infinitely complex patterns, a curve or a time history, exhibit self-similarity across different scales [26]. The dimension of a fractal set is a statistical measure that describes how densely the set occupies the embedding metric space and is measured as a ratio of how the details in the complexity of a pattern changes with the measurement resolution scale. The fractal dimension D is independent of the scale size but depends only on the scaling under changes in the measurement resolution and is a global invariant. In general, the fractal dimension of a fractal set is always larger than its topological dimension but smaller than the dimension of the space in which it is embedded. Thus, for a curve that exhibits fractal characteristics, D is greater than unity but less than 2. This implies that in general D is non-integer. Mathematically, D is defined as *

$$D = \lim_{\epsilon \to 0} \frac{\ln N(\epsilon)}{\ln 1/\epsilon}, \tag{1}$$

where, ϵ is the size of the subdomain of the entire set and represents the resolution scale of the measurements, and $N(\epsilon)$ represents the total number of subdomains that the entire domain of the set can be divided following the resolution scale of the measurements. Sets that exhibit fractal characteristics could also include processes in time. Similar to a fractal curve, a fractal time series also has its dimensions between one and two and possess scale invariance characteristics. It means that a fractal time series comprises of self similar patterns when examined under different scales *i.e.*, the structure of a signal measured for a duration of T units is similar when the same signal is observed for a duration of t units, where $t << T$.

For processes in time that exhibit fluctuations across a wide range of time scales, a single fractal dimension D may not be enough to sufficiently describe the dynamical behaviour. Such processes exhibit structures that vary from one scale to another - segments of the time histories at different scales look alike but are not exactly similar. These time histories are usually characterised by a different fractal dimension depending on the resolution scales of the measurements and are defined as multifractal signals. In characterizing multifractal signals, the focus is not on seeking similarity of the data sets, but the similarity in probability measures associated with these data sets at different scales. This can be explained by dividing the spatial domain of the trajectory into subdomains, and defining a probability measure μ_i associated with each of these subdomains with a singularity index a_i, *i.e.*, $\mu_i \equiv \epsilon^{a_i}$, where, ϵ is the size of the subdomain. Here, the singularity index refers to the power-law divergence behaviour and the probability measure refers to the fraction of time the trajectory spends in the ith subdomain. For a continuous data set $\mathbf{x}$, the point measure μ at $\mathbf{x}$ is defined as

$$D_p(\mathbf{x}) = \lim_{\epsilon \to 0} \frac{\ln \mu(N_\epsilon(\mathbf{x}))}{\ln 1/\epsilon} \tag{2}$$

and is indicative of the fractal dimension given by a_i. Here, $N_\epsilon(\mathbf{x})$ represents a spatial domain with length scale ϵ centred at $\mathbf{x}$ and $\mu(N_\epsilon(\mathbf{x}))$ represents the probability measure expressed as the fractional time spent by the trajectory in $N_\epsilon(\mathbf{x})$. In the limit when $\epsilon \to 0$, one can invoke the continuum assumptions and it can be shown that the scaling exponents a_i are local and continuously distributed in an interval. Further, it can be shown that the number of subdomains $N(\epsilon)$ with singularity index in the range $[a, a + \mathrm{d}a]$ is given by [27]

$$\mathrm{d}N(\epsilon) = \mathrm{d}\mu(a)\epsilon^{-f(a)}, \tag{3}$$

where, $\mu(a)$ is the probability measure of the fractional time spent by the trajectory in a subdomain and $f(a)$ characterises the scaling properties of the local exponent a and is referred in the literature as the singularity spectrum [28, 29, 30].

Since the fractal dimension is indicative of the power law behaviour of the fractal set (or a fractal signal), a quantitative measure of the fractal dimension can be obtained in terms of the moments, whose general expression is given by

$$\chi_q(\epsilon) \sim \int \mathrm{d}\mu(a)\epsilon^{aq-f(a)}, \tag{4}$$

where, $\chi_q(\epsilon)$ is the q-th moment. Further, it can be shown via the asymptotic scaling behaviour of moments [31]

$$\chi_q(\epsilon) \sim \epsilon^{(q-1)D_q}, \tag{5}$$

where, D_q is the generalised fractal dimension. Since the integral in Eq.(4) is valid for small ϵ, the integral is dominated by those values of a which minimises the exponent $[aq - f(a)]$. The integral can therefore be evaluated using the saddle-point approximation [32], leading to

$$D_q = \frac{1}{(q-1)}[\bar{a}q - f(\bar{a})], \tag{6}$$

where,

$$a = \bar{a},\ \frac{\mathrm{d}}{\mathrm{d}a}[aq - f(a)] = 0,\ \frac{\mathrm{d}^2}{\mathrm{d}a^2}[aq - f(a)]|_{a=\bar{a}} > 0. \tag{7}$$

It follows that $\mathrm{d}f/\mathrm{d}a|_{a=\bar{a}} = q(\bar{a})$ and $\mathrm{d}^2 f/\mathrm{d}a^2|_{a=\bar{a}} < 0$. This implies that the $f(a)$ has a convex variation with respect to a, with a maxima at $q = 0$ and an infinite slope at $q = \pm\infty$. Also, Eq.(6) implies that $(q-1)D_q$ and $f(a)$ are Legendre transforms of each other.

For a mono fractal signal, $f(a) = a$. Thus, from Eq.(6) one gets that $D_q = f(a) = D_0$ for all q. On the other hand, for multifractal signals, the generalised multifractal dimension, for a given value of q, is approximated by a uniform fractal whose dimension is $f(a(q))$. Thus, if $f(a)$ is available, one can estimate D_q. Conversely, for a specified D_q, one can find a from the relation

$$\bar{a} = \frac{\mathrm{d}}{\mathrm{d}q}[(q-1)D_q]. \tag{8}$$

For mono-fractal signals, the scaling power law is shown to be related to the Hurst exponent [33]. The Hurst exponent, H, is related to the expected size of changes as a function of the lag τ between observations, and measured by $\mathrm{E}[|X(t+\tau) - X(t)|^2]$, where $\mathrm{E}[\cdot]$ is the expectation operator. The fractal dimension D of a time series is shown to be related as $D = 2 - H$ [34]. The Hurst exponent is related to the scaling properties of a signal. For instance, if $x(t)$ is some fractal signal with Hurst exponent H, then $x(ct) = x(t)/c^H$ is also a fractal signal with the same statistics [35]. A simple approach to provide fractal description of a signal by a technique known as Detrended Fluctuation Analysis (DFA) has been proposed in [36].

For multifractal signals, this concept is generalised [37, 38] through structure functions, which are used to explore the scaling relationships between the variations in the moment of a measured fluctuation and the time interval of measurement [39]. The corresponding generalised Hurst exponents that are estimated describe the scaling in the central moments of the signal that have been appropriately scaled for different positive and negative orders q. Thus, for a multifractal signal, the generalized Hurst exponents vary for different values of q. By carrying out a Legendre transform, the variation in generalized Hurst exponents can be represented by a spectrum of singular peaks $f(a)$.

Early studies on multifractality in measurements have been carried out in the context of turbulence [40, 41, 42]. Subsequently, multifractality of the signals have been investigated in a host of studies involving different engineering disciplines and applications. For example, multifractality of measurements have been used to identify the presence of cracks in rotor systems [43], for fault diagnosis in rotating systems [44], predicting hazardous conditions in complex chemical reactions [45], describing the bifurcation mechanisms in high TC superconducting levitation systems [46], health monitoring of a road bridge [47], short term predictions of atmospheric wind speeds [48], feature extraction from radio transmitter signals [49] and in combustion systems [50, 51, 52, 53]. The present study investigates the multifractality in the aeroelastic response measurements of an airfoil subjected to wind tunnel tests.

3 Wind tunnel experiments

Wind tunnel experiments are carried out in an Eiffel type wind tunnel, at the Bio-mimetic and Dynamics Laboratory, in the Department of Aerospace Engineering, Indian Institute of Technology Madras. The wind tunnel achieves a maximum flow velocity of 25 m/s. A flutter set-up comprising of a pitch and plunge mechanism has been developed for the tests. An explanation of the set-up is provided through the schematic diagram in Fig. 1.

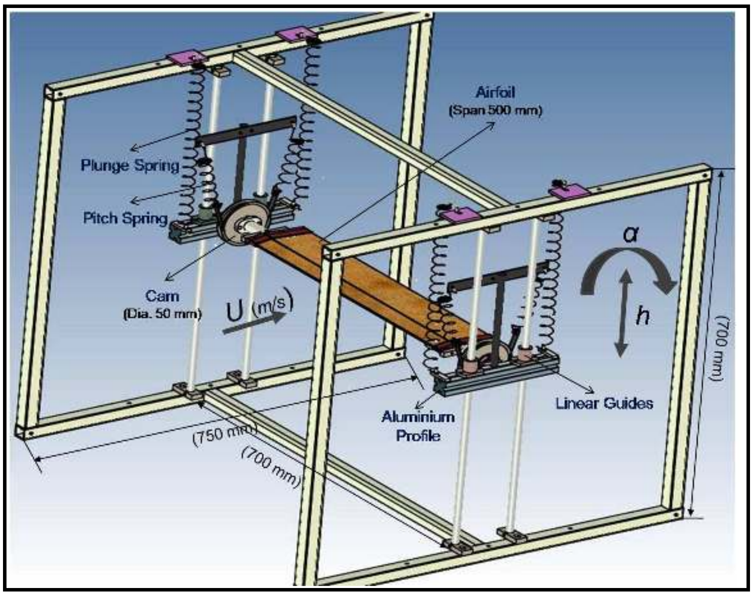

Fig. 1. Schematic of the pitch and plunge apparatus.

A NACA 0012 airfoil having a chord of 100 mm and a span of 500 mm is used for the wind tunnel experiments. The airfoil is horizontally mounted into the flutter setup; see Fig. 2. The

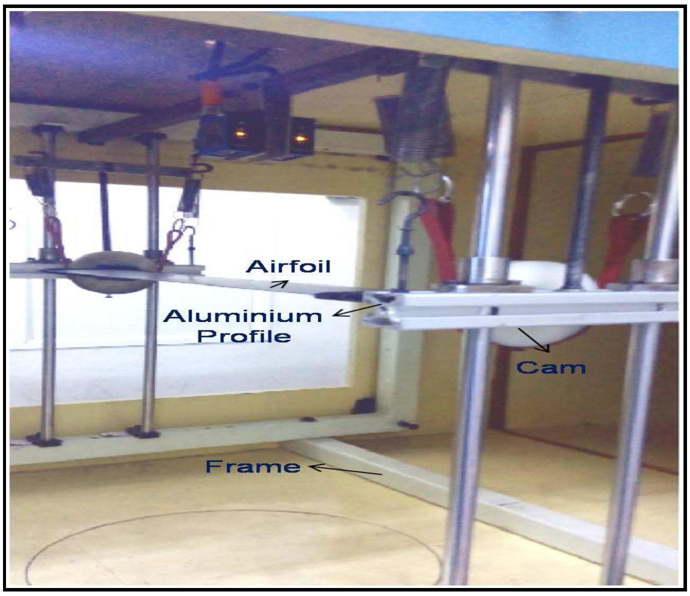

Fig. 2. Photograph of the pitch and plunge apparatus inside the wind tunnel test section.

pitch and plunge mechanism is based on the design in [54] with some modifications. Two identical translation carriages of dimensions 700×750 mm are provided on either side of the test section for plunging. The distance between the two ends is 700 mm. To prevent out-of-plane motions, on each side, the translation carriage has two hardened ground shafts that go through a spring suspended aluminum profile via linear ball bushing-guide ways. Rigidity of the shafts are ensured by fixing the top and bottom ends of the shaft to the support frame using adjustable M4-threaded screws. The pitching motion is enabled through circular a Nylon disc of diameter 50 mm, which is connected to the aluminum profile via linear ball bearings. An industrial Nylon belt is enveloped over the disc and fixed with an M3 screw to the bottom of the disc. The belt has provision for spring suspension and thus the spring suspended disc is used for obtaining rotary motion. A slot is provided in the disc to attach a steel gripper, of length 100 mm. The gripper consists of an adjustable steel bar with a hollow pocket to attach the airfoil into it. Grub screws are used to fix the airfoil firmly into the pocket. The position of the elastic axis is identified by changing the location of the pocket over the adjustable steel bar and tightening the grub screw.

The entire set-up is placed inside the wind tunnel; see Fig. 2. All the experiments were conducted under blowing conditions of the wind tunnel fan so as to create realistic environmental conditions as opposed to sterile flow conditions when the tunnel is operated under suction mode. A pitot tube manometer is placed on the upstream of the test section to measure the flow speeds. Measurements of the airfoil displacements are obtained by using a pair of Wenglor Opto NCDT type laser sensors, each having measurement range of 300 mm. Signals from the laser sensors are acquired using a 4-channel ATALON data acquisition system having an input voltage of $\pm$ 5 V and 24-bit resolution. The measured response was acquired with a sampling rate of 5024. The airfoil response measurements are acquired for a duration of 120 seconds corresponding to different flow speeds. The flow speeds were varied in the range of $4-8$ m/s in steps of 0.4 m/s. A Delta HD 4V3 TS3 air velocity sensor is used to measure the flow velocity inside the test section. It measures the instantaneous changes in the air velocity at a specified location and has a measurement range of 0-40 m/s. The ATALON data acquisition system is used for measuring the flow velocity also. The initial angle of attack of the airfoil is set to zero degrees. Tests were carried out to identify the physical parameters associated with the experimental set-up and these are listed in Table 1.

m_1	m_2	m_3	m_y	m_α	I_α	k_y	k_α	S	c_y	c_α
1.1	0.9	0.4	2.4	1.3	0.007	1800	6.29	0.006	6.758	0.012
Kg	Kg	Kg	Kg	Kg	Kg-m^2	N/m	Nm/rad	Kg-m	Kg/s	Kg-m$^2/s$

Table 1
Physical parameters of the experimental setup.

Here, m_1 is mass of plunging frame , m_2 is mass of pitching mechanism, m_3 is mass of airfoil, m_y is total mass in plunge, m_α is total pitching mass, c is the airfoil chord length, I_α is the pitch moment of inertia, K_y is the stiffness in plunge, K_α is stiffness in pitch, c_y is the viscous damping coefficient in plunge, c_α is viscous damping coefficient in pitch and S is the static unbalance. The heaving motion in the setup is controlled by the four plunge springs, while the pitching motion is controlled by the four pitch springs along with the circular cam. The nonlinearity in the pitch can be controlled by changing the geometry of the cam. A force deflection curve obtained from a controlled pitching motion alone revealed that the pitching stiffness remained linear. However, the force deflection curve revealed the heaving stiffness can be approximated as a cubic nonlinearity. The damping associated with the system is modelled to be viscous and the coefficients of viscous damping along the pitch and plunge directions were estimated from measuring the free vibration response and using the standard logarithmic decay technique.

4 Results and discussion

Wind tunnel tests were carried out by gradually increasing the flow speed in the test section and monitoring the airfoil response for each wind speed. Figure 3 shows segments of the response measurements along the plunge and the pitch degrees of freedom for flow speed $U = 4$ m/s (left column) and $U = 8$ m/s (right column). At $U = 4$ m/s, the time histories of the response for both plunge and pitching degrees of freedom are observed to comprise of low amplitude aperiodic segments; see Figs. 3a and 3c. This is confirmed from the broad band nature of the spectrum for the respective time histories; see Figs. 3e and Fig. 3e for plunge and pitch respectively. On the other hand, when U is increased to 8 m/s, the response measurements are observed to comprise of large amplitude periodic oscillations indicating the onset of aeroelastic flutter; see Figs. 3b and 3d for the time histories for plunge and pitch. The corresponding spectrum representation are respectively shown in Figs. 3f and Fig. 3h. These figures reveal a dominant frequency confirming a predominant oscillatory mation and characteristics of post-flutter hevaior. The variations of plunge and pitch dominant frequencies with wind speed are shown in Fig. 3i and Fig. 3j. As the wind speed is continuously increased there is a linear rise in these frequencies.

A closer inspection of the time histories at $U = 4$ m/s, and confirmed by the spectrum shown in Figure 3e reveals the aperiodic oscillations to be similar to a broad banded noise. Studies in the literature have dismissed these type of measurements to be noisy. However, these “noisy” measurements are now investigated for multi-fracatal characteristics. The generalised Hurst

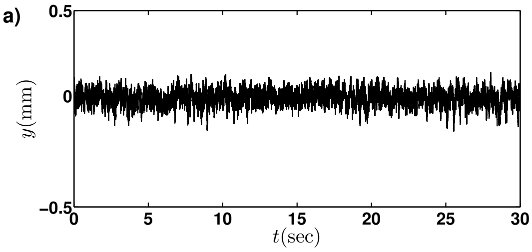

(a) Plunge; $U = 4$ m/s.

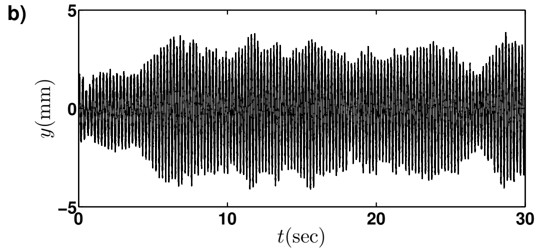

(b) Plunge; $U = 8$ m/s.

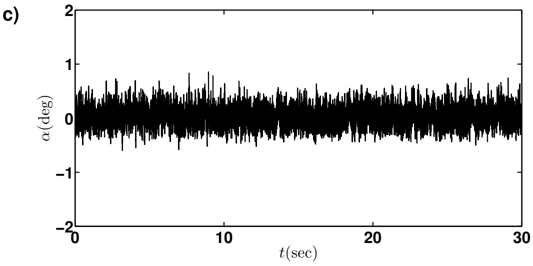

(c) Pitch; $U = 4$ m/s.

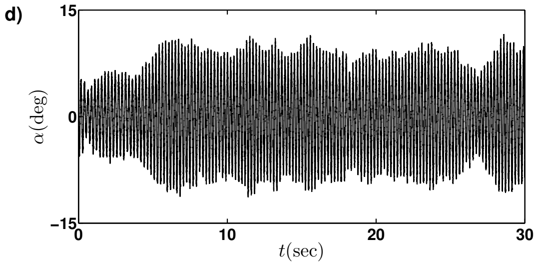

(d) Pitch; $U = 8$ m/s.

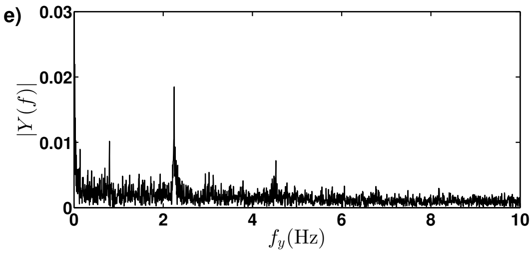

(e) Spectrum for plunge; $U = 4$ m/s.

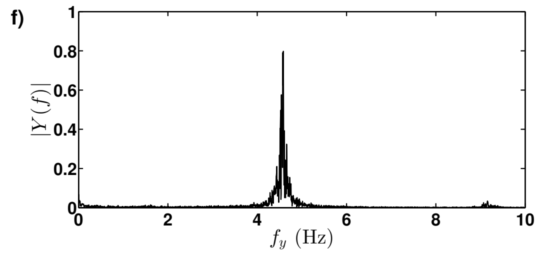

(f) Spectrum for plunge; $U = 8$ m/s.

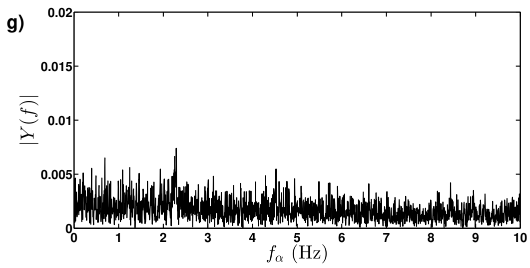

(g) Spectrum for pitch; $U = 4$ m/s.

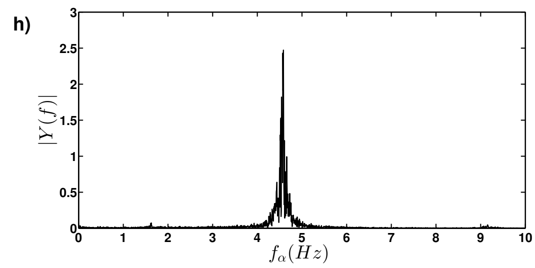

(h) Spectrum for pitch; $U = 8$ m/s.

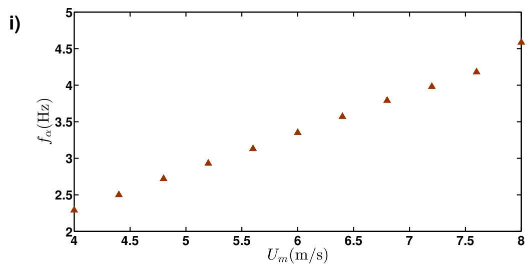

(i) Variation of plunge response frequency with wind velocity

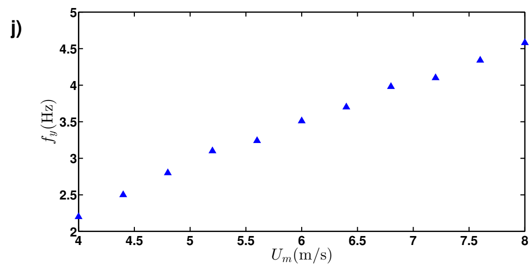

(j) Variation of pitch response frequency with wind velocity

Fig. 3. Measured airfoil responses in plunge and pitch degrees of freedom along with the spectral representation for a flow speed $U = 4$ m/s (first column) and for $U = 8$ m/s (second column).

exponents are now estimated for the time history measurements corresponding to $U = 4$ m/s and $U = 8$ m/s and are shown in Figure 4. The algorithm for computing the generalised Hurst

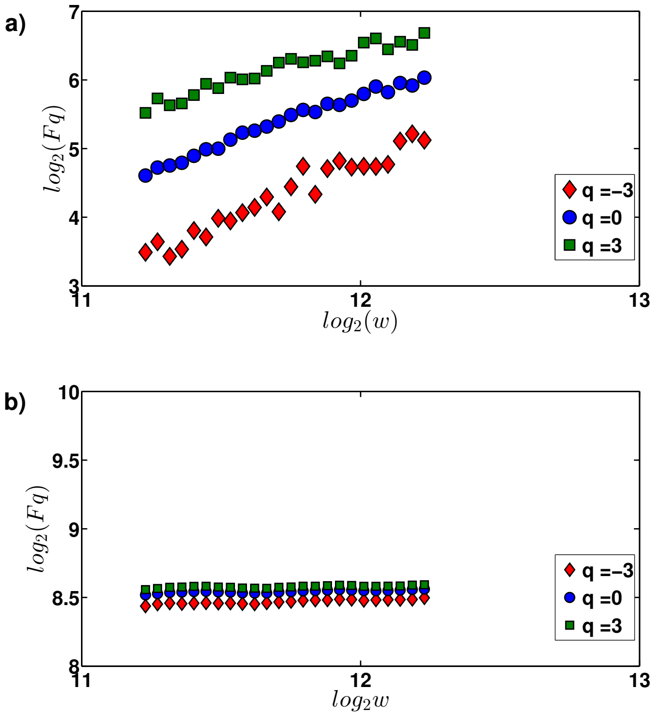

Fig. 4. The variation of structure function F_q with time intervals w, at different orders q; (a) $U = 4$ m/s, (b) $U = 8$ m/s.

exponents are adopted from the study carried out in [53] and is detailed in the appendix for the sake of completion. By varying the order exponent q, high and low amplitude fluctuations in different time intervals w are preferentially selected. While positive values of q amplified the effects of high amplitude fluctuations, negative values of q amplifies the low amplitude fluctuations.

Figure 4a shows the variation of the structure functions F_q for $U = 4$ m/s for q equal to -3, 0 and 3. Here, the slopes of these lines give the generalised Hurst exponent of order q and denoted by H. Structure function gives the scaling properties between the variations in the moments of measured time series and the time interval of the measurement [38, 39]. The intervals w are chosen based on identifying the regimes in which the Hurst exponent is almost zero. In a recent study [55], it has been shown that in 2-4 cycles of the time history the Hurst exponent remains close to zero and hence the intervals w were chosen accordingly. It is observed that the slopes for the variation of the structure functions F_q for various values of q are different, indicating the multi fractal natter of the measurements [38]. If the signal was mono-fractal, the generalized Hurst exponents would have been identical for different values of q, the slopes of the lines in Figure 4a would have been identical and the lines would have been parallel. Figure 4b shows the variation of F_q as a function of w, computed for the measurements obtained when $U = 8$ m/s. It is observed that there is almost zero variation of the structure functions with respect to w indicating the slopes to be almost zero. Also, changing q does not lead to different estimates because the existence of LCOs indicate just a single time scale being associated with these measurements. Thus, post flutter, the fractal nature of the measurements is almost lost.

Figure 5 presents the multifractal spectrum of the measured aeroelastic responses at $U = 4$ m/s and $U = 8$ m/s. The singularity spectrum obtained for response measurements taken at $U = 4$ m/s and shown in Figure 5a reveals a broad band profile implying the presence of several exponents and thus, the multifractal nature of the response. On the other hand, the corresponding singularity spectrum obtained from response measurements once LCO has set in and shown in Figure 5b reveals a clustering around zero. This indicates a lack of scale invariance post flutter when the response is characterised by LCO.

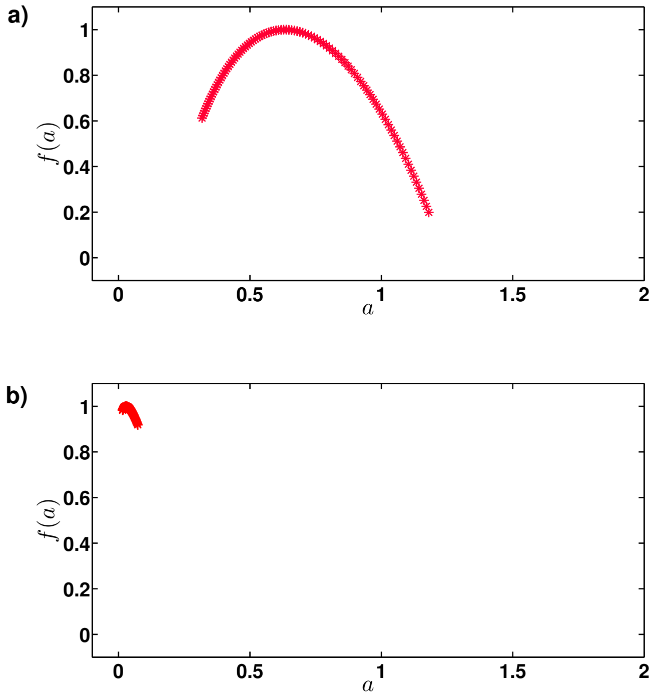

Fig. 5. Variation of singularity spectrum $f(a)$ with singularity strength a, which is equivalent to the Hurst exponent, for, a) the multifractality present in the response at $U = 4$ m/s and b) its collapse post flutter at $U = 8$ m/s.

5 Precursor to aeroelastic flutter

Loss of multifractal signature at the onset of flutter instability can be used to successfully predict the onset of impending instability. The gradual drop in Hurst exponent H as flutter is approached can be used as a precursor to an impending flutter. Traditionally, characterisation of measurement signals is carried out in terms of the root mean square (r.m.s.) values and are computed as

$$y_{rms} = \left\{ \frac{1}{N} \sum_{i=1}^{N} y_i^2 \right\}^{1/2}. \tag{9}$$

Here, y_i indicates the measured response $y(t)$ at $t = t_i$, corresponding to a particular flow speed U, and N is the total number of measurements. The variation of the r.m.s. values computed from the measured time histories corresponding to different flow velocities U is shown in Figure 6a. It is observed that y_{rms} is almost steady in the range of U from $4-6.5$ m/s and shows a sharp increase for flow speeds beyond 7.5 m/s. This seems to indicate that the growth in y_{rms} values corresponds to the onset of LCO. Note that an inspection of the time histories of the response at $U = 8$ m/s indicates that LCO has already set in at this flow speed. Thus, y_{rms} can only convey the manifestation of an oscillatory instability, that has already begun, rather than forewarning an impending instability.

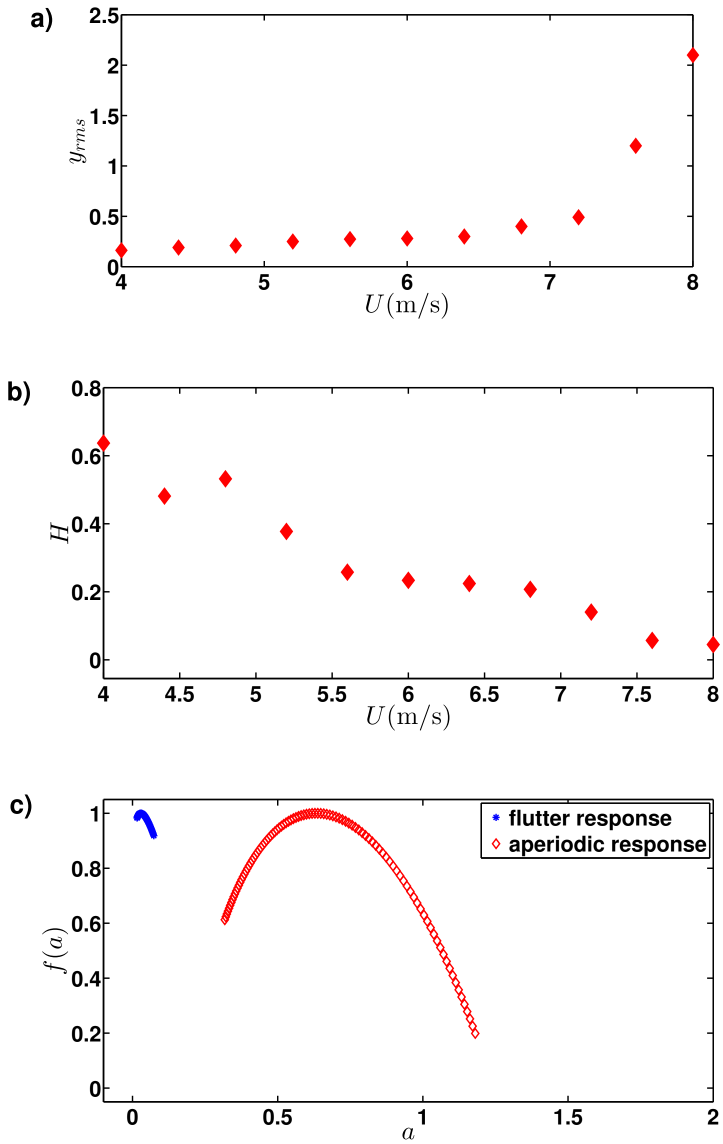

Fig. 6. Variation of r.m.s value of airfoil response and Hurst exponent with flow speed are shown in a) and b) respectively. The loss in multifractality is shown in figure c).

Figure 6b shows the variation of the Hurst exponent computed from the response measurements corresponding to various flow speeds U. A visual inspection of the variation reveals that a smooth drop in the magnitude of Hurst exponent H is observed from $U \approx 5$ m/s. It is to be noted that large amplitude oscillations in the airfoil is encountered only after $U > 7.5$ m/s, whereas the developed precursor shows a gradual drop in its magnitude right from regimes of stable operating conditions. Moreover, it is clear that the Hurst exponent is close to zero in the presence of LCO. Therefore, by choosing an appropriate threshold for H, away from but close to zero, an operator working with large ordered aeroelastic structures can adopt suitable control measures, so as to prevent the system from transgressing into the regimes of instability.

The loss of multifractal signature at flutter onset can be seen in the singularity spectrum shown in Figure 6c. The spectrum $f(a)$ diminishes to a point at the onset of flutter instability. This loss in multifractal characteristic could be due to the presence of a single dominant time scale that dictates the dynamics post flutter. Such a loss in the variability in scales is known as "loss of spectral reserve"[56]. In the aeroelastic problem considered here, the loss of spectral reserve takes place in a smooth and gradual manner when the flow speed is gradually increased to the regimes of instability.

It is worth emphasising here that the approach to develop precursor in this study is based on experimental measurements only. Existing studies in the aeroelastic literature involving the development of precursors are based on developing mathematical models for the system and carrying out an analysis. This is not a trivial problem as developing a mathematical model for a highly complex fluid-elastic problem is fraught with difficulties and require solving an inverse problem first to ensure correct identification of the various parameters that enter the mathematical model. Moreover, structural systems under operating conditions undergo material and structural degradation that alters the model parameters with time, which in turn changes the stability boundaries. This implies that a model updating exercise needs to be carried out at regular time intervals. On the other hand, the present approach is based on investigating the multifractal characteristics of the response measurements and bypasses the need for developing mathematical models for the system. Moreover, even if the stability boundaries undergo changes with time due to the gradual structural degradation, the proposed approach would still be able to identify the stability boundaries by studying the signatures of the response measurements. Thus, the proposed approach is suitable for online health monitoring for a number of aeroelastic applications, such as, aircraft wings, blades of wind turbines, rotor blades, helicopter blades and other similar applications.

6 Model independence

It must be reemphasized here that the precursors developed here are model independent. A model free method to predict instabilities has distinct practical advantages over a model dependent approach. A primary difficulty with model based approaches to predicting the stability boundary lies in developing an accurate mathematical model for the system. Any uncertainties in developing the model propagate through the analysis and leads to predictions of the stability boundaries, which are itself uncertain. Additionally, due to the effect of ageing, the structural parameters usually degrade with time. This leads to changing of the stability boundaries with time. Unfortunately, mathematical models for ageing of structural components are not as well developed and hence significant epistemic uncertainties are introduced into the formulation when ageing effects are incorporated into the mathematical model. In real life applications, it is expected that both these uncertainties exist. For assessment of the stability boundaries using model dependent techniques, therefore, require accurate identification of the system parameters of the mathematical model. Hence, solving expressed as

$$
\begin{aligned}
m_y\ddot{y} + m_3 b x_\alpha \ddot{\alpha} + k_y y + L &= 0, &(10)\\
m_3 b x_\alpha \ddot{y} + I_\alpha \ddot{\alpha} + k_\alpha \alpha - L(0.5 + a_h)b &= 0. &(11)
\end{aligned}
$$

Here, for steady flow conditions,

$$L = 2\pi\rho U^2 b\alpha, \tag{12}$$

and for quasi-steady flow conditions,

$$L = 2\pi\rho b U^2\Big(\alpha + \frac{\dot{y}}{U} + (0.5 - a_h)\frac{b\dot{\alpha}}{U}\Big). \tag{13}$$

Note that in accordance with the thin airfoil theory, the lift slope is taken to be 2π. Using the notation for the uncoupled natural frequencies as $\omega_y = k_y/m_y$ and $\omega_\alpha = k_\alpha/I_\alpha$, and a nondimensional frequency parameter $p = \nu b/U$ with ν as the flutter frequency, an eigenvalue form can be obtained. The other nondimensional parameters are: radius of gyration $r = \sqrt{I_\alpha/m_\alpha b^2}$, ratio of plunge and pitch natural frequencies $\varpi = \omega_y/\omega_\alpha$, non-dimensional mass $\mu = m_y/\pi\rho b^2$, non-dimensional wind speed $V = U/b\omega_\alpha$, non-dimensional distance between elastic axis and centre of mass $x_\alpha = S/m_\alpha b$, non-dimensional distance between mid chord of airfoil to elastic axis a_h, viscous damping ratio in plunge ζ_y and viscous damping ratio in pitch ζ_α. Here, $y = \bar{y}\exp(\nu t)$ and $\alpha = \bar{\alpha}\exp(\nu t)$. The eigenvalue problem for the steady flow conditions can be expressed as

$$\begin{bmatrix} p^2 + \frac{\varpi^2}{V^2} & \frac{m_3}{m_y}x_\alpha p^2 + \frac{2}{\mu} \\ \frac{m_3}{m_y}x_\alpha p^2 & \frac{m_\alpha}{m_y}r^2p^2 + \frac{m_\alpha}{m_y}\frac{r^2}{V^2} - \frac{2}{\mu}(a_h + 0.5) \end{bmatrix} \begin{Bmatrix} \frac{\bar{y}}{b} \\ \bar{\alpha} \end{Bmatrix} = \begin{Bmatrix} 0 \\ 0 \end{Bmatrix}. \tag{14}$$

The corresponding eigenvalue problem for the quasi-steady flow conditions is expressed as

$$[A]\begin{Bmatrix} \frac{\bar{y}}{b} \\ \bar{\alpha} \end{Bmatrix} = \begin{Bmatrix} 0 \\ 0 \end{Bmatrix}. \tag{15}$$

where the matrix $[A]$ is a 2×2 matrix of the form

$$\begin{bmatrix} p^2 + \frac{2p}{\mu} + \frac{\varpi^2}{V^2} & \frac{m_3}{m_y}x_\alpha p^2 + \frac{2p}{\mu}(0.5 - a_h) + \frac{2}{\mu} \\ \frac{m_3}{m_y}x_\alpha p^2 - \frac{2p}{\mu}(a + 0.5) & \frac{m_\alpha}{m_y}r^2p^2 - \frac{2p}{\mu}(a_h + 0.5)(0.5 - a_h) + \frac{m_\alpha}{m_y}\frac{r^2}{V^2} - \frac{2}{\mu}(a_h + 0.5) \end{bmatrix}. \tag{16}$$

The eigenvalues obtained from Eqs.(14-15) typically constitute a complex conjugate pair of roots of the form

$$
\begin{aligned}
p_1 &= \Gamma_1 \pm \mathrm{i}\Omega_1,\\
p_2 &= \Gamma_2 \pm \mathrm{i}\Omega_2. &(17)
\end{aligned}
$$

The behaviour of these complex roots with wind speed (U) can be used to verify the onset of flutter instability [59]. Figure 8 shows the variation of the real and imaginary components of these eigenvalues, for both the steady and the quasi-steady cases.

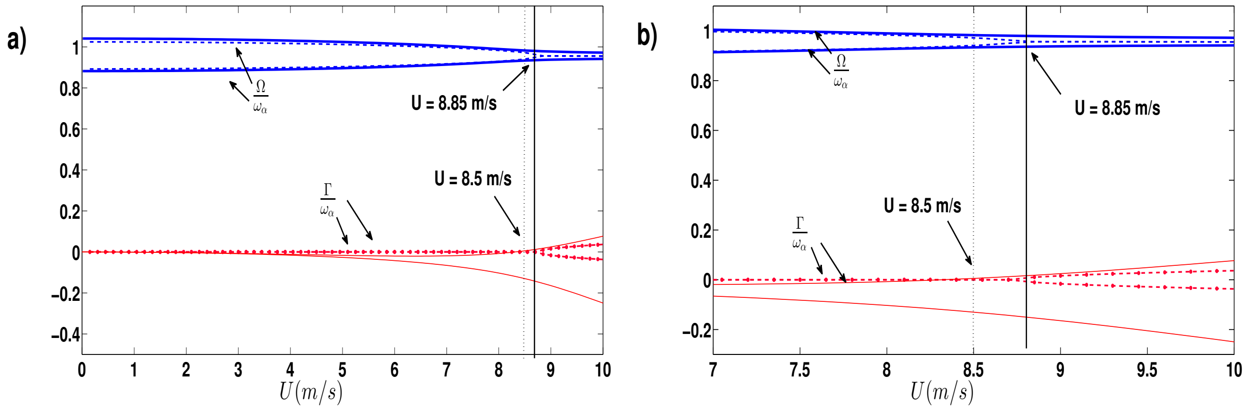

Fig. 8. a) Variation of real (modal damping) and imaginary parts (modal frequency) of solution of Eqs. 14 and 15 with airspeed. The dashed lines correspond to steady aerodynamics and the solid ones correspond to quasi steady aerodynamics and b) Zoomed view of figure a). The dashed blue line correspond to imaginary part of solution from steady state aerodynamics and the dashed red line represent the corresponding real part. The solid blue line represent the imaginary part of solution obtained using quasi-steady aerodynamics and the red solid lines represents the corresponding real part.

In steady flow condition, the onset of flutter is identified by the coalescence of the imaginary components of the eigenvalues (dashed lines without markers) and is seen to occur at $U = 8.85$ m/s. When the flow is quasi-steady, the onset of flutter is characterized as when the modal damping, denoted by the real part of the eigenvalues, changes from zero to a positive value indicating divergence and is seen to occur at $U = 8.5$ m/s; see the full line with markers. More details on the theory behind this is available in [59] and is not repeated here.

In the case of unsteady aerodynamic modelling, the loads are expressed in terms of the following intego-differential form [1],

$$
\begin{aligned}
L(t) = {} & 2\pi\rho b U^2[\alpha(0) + \frac{\dot{y}(0)}{U} + \frac{b}{U}(0.5 - a_h)\dot{\alpha}(0)]\phi(t) \\
& + 2\pi\rho b U^2 \int_0^t \phi(t - t_0)[\dot{\alpha}(t) + \frac{\ddot{y}(t)}{U} + \frac{b}{U}(0.5 - a_h)\ddot{\alpha}(t)]\mathrm{d}t_0. \qquad (18)
\end{aligned}
$$

The time function $\phi(\tau)$ is the Wagner's function which can be approximated as [60]

$$\phi(\tau) = 1 - 0.165\exp(-0.0455\tau) - 0.335\exp(-0.3\tau). \qquad (19)$$

The integro-differential equations are numerically integrated following the procedure adopted in [57]. From the bifurcation diagram obtained numerically and shown in Fig. 9, it can be seen that the onset of LCO occurs at $U = 8.35$ m/s via a supercritical Hopf bifurcation.

The physical parameters estimated from the experimental set-up were given in Table 1; the corresponding nondimensional values used here for the numerical analysis are listed in Table 2. Note that fully developed LCO's were observed in the experiments at approximately $U = 8$ m/s. However, as has been mentioned earlier in Section 3, the flow in the wind tunnel was not uniform but was accompanied by fluctuations.

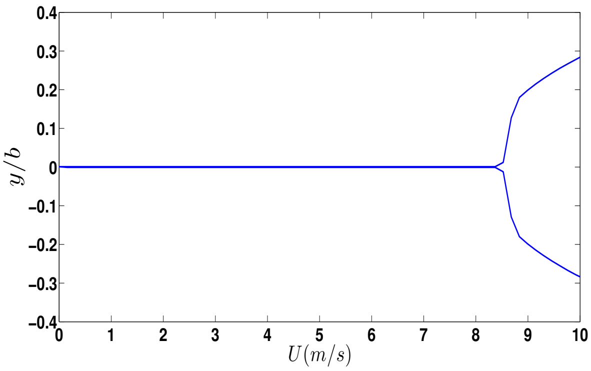

Fig. 9. Bifurcation diagram of the response as a function of U.

r	μ	x_α	a_h	ζ_α	ζ_y	ϖ
0.707	660	0.3	-0.5	0.03	0.05	0.91

Table 2
Non-dimensional parameters of the experimental setup

So far in the numerical calculations, the flow has been assumed to be uniform and without any fluctuations. In such sterile conditions, the multifractal signature that has been observed in the experiments cannot be seen. In real life scenario, the flow is usually accompanied by fluctuations arising due to various causes. These fluctuations need to be incorporated into the mathematical model for further analysis.

As no quantitative measurements of the fluctuations in the flow were available due to lack of appropriate hardware such as Laser Doppler Velocimetry (LDV) or Particle Image Velocimetry (PIV). it was decided to use a simple canonical model that captures the inherent characteristics of turbulent flows. Studies have shown that [40, 61] turbulent flows involve multiple time scales. Thus, in this study a canonical model of the form (see Eq. 20)

$$V = \frac{U_m}{b\omega_\alpha}(1 + \sigma(\sin(\omega_{r1}t) + \sin(\omega_{r2}t) + \sin(\omega_{r3}t))), \tag{20}$$

was considered for the flow fluctuations. Here, U_m is the dimensional mean wind speed in m/s, σ indicates the amplitude of the fluctuating component and $b\omega_\alpha$ has the same meanings as mentioned in the manuscript. The frequency of the sinusoids are expressed as $\omega_{r_i} = \omega_i + \kappa R_i$, $(i = 1, 2, 3)$, where, R_i, are uniformly distributed random numbers lying between $[0, 1]$ and κ is a constant having a small value. The three frequencies ω_1, ω_2 and ω_3 have been taken to be arbitrary but incommensurate with each other to avoid periodicity in both short or long time scales. The small fluctuations κR_i, $(i = 1, 2, 3)$, have been added to the frequency of the sinusoids at each time increment to mimic the random nature of the fluctuations in the flow. Note that the spectral representation of a random process involves the linear superposition of a large number of sinusoids [62] and the use of random process models for fluctuating wind flows have been used in aeroelastic literature [17]. However, this requires the knowledge of the power spectral density function as well as the probability density function of the process, neither of which is available in the present case. The use of the simple canonical model shown in Eq. (20) however serves the necessary purpose of introducing additional time scale that arise due to turbulence in the flow. A similar canonical form for modelling the flow fluctuations has been used recently in [22].

The time histories of the plunge response non-dimensionalized by semi-chord, for various wind speeds are obtained by numerical integration and are shown in Fig. 10. As U_m is gradually increased, low amplitude aperiodic fluctuations are observed; see Fig. 10(a). This behaviour is qualitatively similar to the observations from wind tunnel experiments. Finally, well developed LCO are obtained on further increasing U_m; see Fig. 10(b).

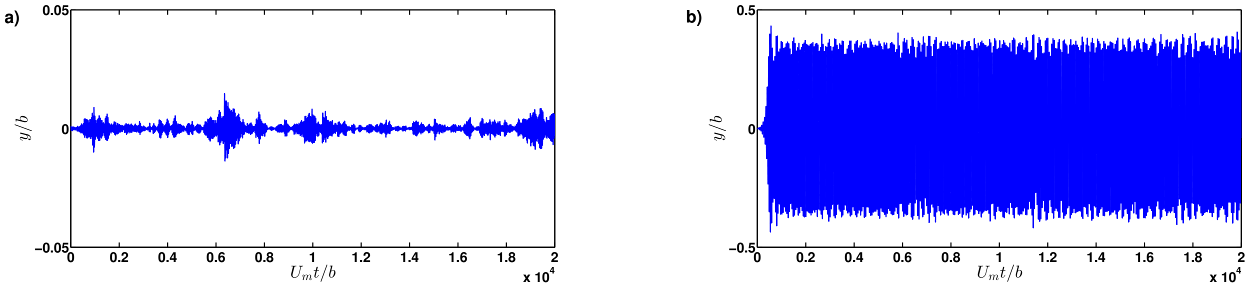

Fig. 10. Non-dimensionalized plunge response from numerical model; a) $U_m = 4$ m/s and b) $U_m = 8$ m/s.

The multifractal spectrum for the numerically generated time series is shown in Figure 11. In the case when $U_m = 4$ m/s, the singularity spectrum is broad band and indicates the

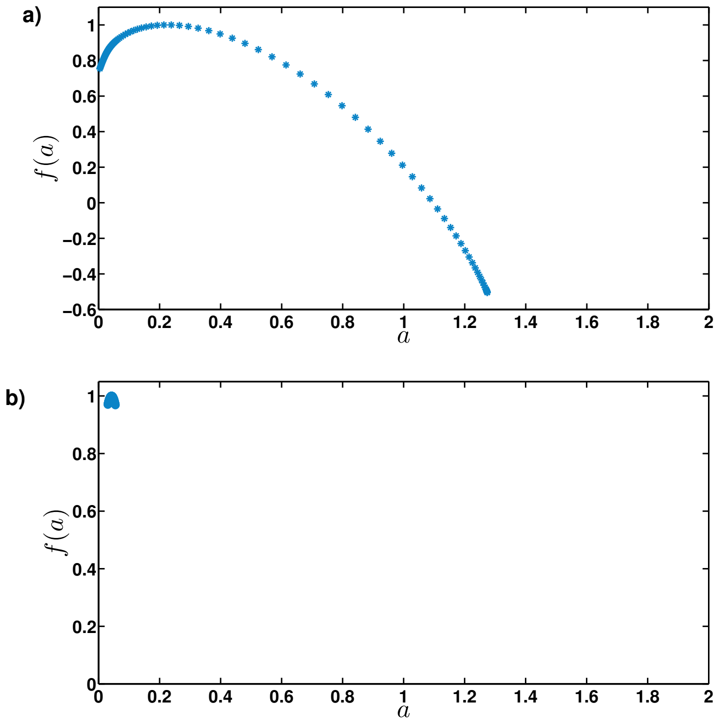

Fig. 11. Variation of singularity spectrum with strength a for the numerical data at; a) $U_m = 4$ m/s and b)$U_m = 8$ m/s.

presence of a range of exponents, thus revealing the multifractal signature present in the data. As flutter is approached, the spectrum collapses into a small region clustered around zero, indicating that the fluctuations happen only at a single time scale, indicating a loss of multifractal behaviour. In the presence of fluctuations in the flow, the system response never attains complete rest even in regions to the left of the bifurcation point shown in

Fig. 10. The multifractal nature of the response is due to the overwhelming effect of the turbulence in the flow, leading to a higher Hurst exponent. For the region to the right of the bifurcation point, the system in sterile flow exhibits periodic oscillations; in the presence of fluctuating flows, these oscillations are superimposed with fluctuations. The amplitudes of the noisy response therefore have significant contributions from the oscillations which are superimposed by small fluctuations due to the fluctuations in the flow. Thus, the dynamic behavior is more regular in this region leading to low Hurst exponent value but not equal to zero. Note that the Hurst exponent of a regular periodic signal is zero.

To check the robustness of the precursor proposed in this paper, these synthetically generated time histories are next used to forecast an impending aeroelastic flutter using the proposed fractal analysis. Figure 12(b) show the variation of Hurst exponent with mean wind speed U_m. The non-dimensional r.m.s. value of response is plotted in Figure 12(a). An inspection of

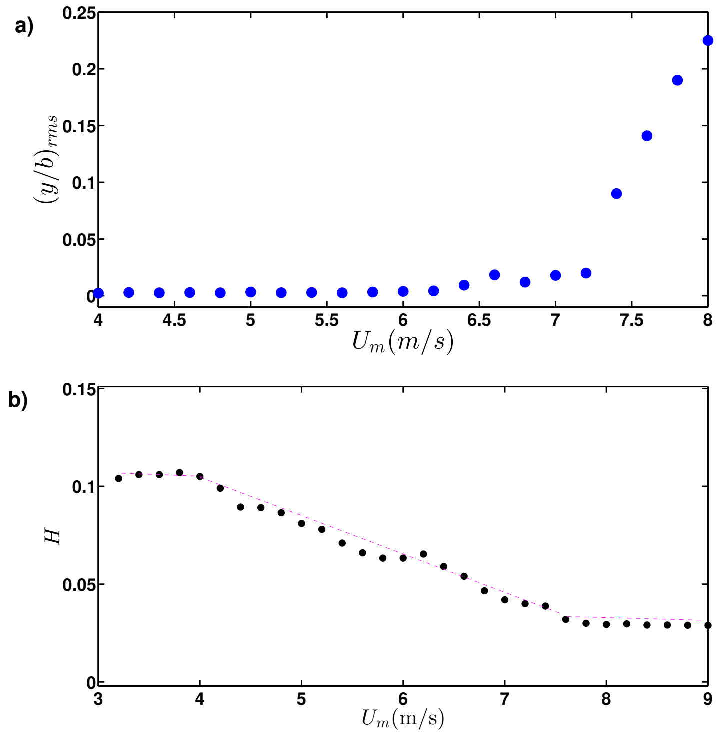

Fig. 12. a)The rms of the numerically generated response with wind speed and b) Gradual drop in magnitude of H as the wind speed is increased towards flutter conditions.

Fig. 12(b) reveals that the Hurst exponent has an almost constant value for $U_m < 4$ m/s and there is a distinct change in the slope of the variation of the Hurst exponent from $U_m = 4$ m/s. The Hurst exponent gradually decreases till about $U_m = 7.8$ m/s and beyond that attains a constant value of about 0.03. Further increasing U_m does not lead to a lower value of the Hurst exponent. As Fig. 10(b) reveals, the oscillations are already well developed at $U_m = 8$ m/s. In the presence of fluctuating flows, unlike in the case of sterile flows, one cannot define a sharp boundary between the two stability regimes. Instead, the boundary is now more diffused and the response in these regions is characterized by intermittent behavior. The time histories of the response are characterised by irregular bursts of small and high amplitude oscillations. The presence of irregular bursts of large amplitude oscillations imply that the Hurst exponent would be now lower than in regimes where the response is characterized by small but noisy fluctuations. Thus, the onset of the instability regime can be identified when the Hurst exponent starts decreasing from a more or less constant value, as the bifurcation parameter is gradually changed.

Figure 12(b) clearly shows that the Hurst exponent starts decreasing prior to the onset of LCO and can be used as a precursor. This is in contrast to the variation of y_{rms} shown in Fig. 12(a), where there is an appreciable change only *after* the onset of oscillatory motion. In usual engineering applications, the safe operating principles associated with the system demands that the system does not venture into the LCO regime. The online monitoring of the response measurements and calculation of the Hurst exponent provides an important metric which will enable the engineer in charge of the safety of the system to take decisions when to take remedial measures; the choice of the threshold numerical value of H depends on the desired safety margin and is usually a policy decision.

The figures obtained from analysis of the experimental observations also reveal a similar drop in the Hurst exponent from a value of about 0.5 to values close to zero as U is increased; see Fig. 6(b). Experimental measurements are not available for $U < 4$ m/s and hence the behavior of the Hurst exponent at $U < 4$ m/s could not be investigated. However, a qualitatively similar variation in the Hurst exponent is observed from both experimental and numerical measurements. Quantitatively the Hurst exponent is higher in experimental measurements; this can be attributed to a wider spectrum bandwidth for the fluctuations in the flow.

Thus the numerical investigations presented in this section provides a qualitative validation to the observations obtained from the wind tunnel experiments. Importantly, the numerical investigations confirm that the precursor proposed in this study are effective in providing an early warning to the onset of aero-elastic flutter in the presence of flows with small fluctuating components. The necessity for the flow to have fluctuations is not unrealistic as in field conditions, the flow will not be sterile and be usually accompanied by small fluctuations due to the interactions with the structure and its various components.

8 Concluding remarks

The transition from low-amplitude, aperiodic fluctuations to fully developed flutter instability in an airfoil has been investigated experimentally through wind tunnel tests. The irregular fluctuations observed in the response in pre-flutter regimes is shown to posses multifractal characteristics. As the flow speed is gradually increased and the system approaches flutter instability, the fractal characteristics in the flow are observed to weaken and are finally destroyed once limit cycle oscillations set in. This loss of spectral reserve can be used as a precursor to an impending flutter instability.

The possible reasons for the existence of multifractal characteristics in the response is possibly due to the small scale turbulent effects due to the operation of the wind tunnel under blowing conditions. Though, quantifying the turbulence is out of scope in this present study, it can be qualitatively said that the turbulent fluctuations could have given rise to multiple time scales in the airfoil response In flow regimes far away from flutter, these small scale local fluctuations affect the response leading to the multifractal characteristics. As the system approaches the instability boundaries, the effect of these local fluctuations become weaker as the structure and fluid damping approach closer. The onset of flutter is characterised by the system losing stability leading to large amplitude periodic oscillations and the effects of the small scale fluctuations in the flow become negligible. This can be easily observed from an inspection of the scales in the y-axis of the time histories shown in Figure 12. An impending flutter instability is forewarned by a smooth drop in the magnitude of Hurst exponent (H). A suitable user specific threshold for H can defined so as to track the proximity of the aeroelastic system to flutter and take necessary control measures. The presence of fluctuations in the flow is however, of practical significance as in reality, not only wind flows are naturally accompanied with fluctuations, the presence of various adjoining structural components additionally induces small scale fluctuations in the flow.

A Evaluation of generalised Hurst exponents and the multi fractal spectrum

The steps involved in the computation of the generalised Hurst exponents using DFA are summarised as follows:

(1) First, the time history of the measured response $y(t)$ of length N is mean adjusted and a cumulative deviate series y_k is obtained as

$$y_k = \sum_{i=1}^{k}(y(t) - m), \tag{A.1}$$

where, m is the temporal average given by

$$m = \frac{1}{N}\sum_{i=1}^{N} y(t). \tag{A.2}$$

(2) The deviate series is further subdivide into n_w non-overlapping segments of equal span w. For removing the trends in the segments, a local linear fit $\bar{y}_i$ is made to the deviate series y_i and the fluctuations are obtained by subtracting the linear fit from the deviate series.

(3) The structure function of order q and denoted by F_q is computed from the detrended fluctuations as

$$F_q = \left(\frac{1}{n_w}\sum_{i=1}^{n_w}\sqrt{\frac{1}{w}\sum_{j=1}^{w}(y_i - \bar{y}_i)^2)}^{\,q}\right)^{1/q}. \tag{A.3}$$

For $q = 0$, the structure function is defined as

$$F_0 = \exp[\frac{1}{2n_w}\sum_{i=1}^{n_w}\log\left(\frac{1}{w}\sum_{j=1}^{w}(y_i - \bar{y}_i)^2\right)]. \tag{A.4}$$

(4) The Hurst exponent H is the slope of the linear regime on a logarithmic plot of F_2 for various span sizes w. Similarly, the generalised Hurst exponent H_q are the slopes of the linear regime of $\log F_q$ of various orders of q versus $\log w$.

The singularity spectrum $f(a)$ can be obtained from H_q through a Legendre transform, through the following set of equations:

$$\tau_q = qH_q - 1 \tag{A.5}$$

$$a = \frac{\partial \tau_q}{\partial q} \tag{A.6}$$

$$f(a) = aq - \tau_q. \tag{A.7}$$

The plot of $f(a)$ versus a is known as the multi fractal spectrum or the singularity spectrum.

References

[1] Y. Fung, An Introduction to the Theory of Aeroelasticity, Wiley, New York (1955).

[2] B. H. K. Lee, L. Jiang, Flutter of an airfoil with cubic restoring force, Journal of Fluids and Structures 13 (1999) 75–101.

[3] H. Alighanbari, S. J. Price, The post-hopf-bifurcation response of an airfoil in incompressible two-dimensional flow, Nonlinear Dynamics 10 (1996) 381–400.

[4] A. Hauenstein, J. Zara, W. Eversman, I. Qumei, Chaotic and nonlinear dynamic response of aerosurfaces with structural nonlinearities, AIAA Journal 92 (1992).

[5] C. H. Gilliat, T. Strganac, A. Kurdila, An investigation of internal resonance in aeroelastic systems, Nonlinear Dynamics 31 (2003) 1–22.

[6] D. Cox, H. C. J. Curtiss, J. W. Edwards, K. C. Hall, D. A. Peters, R. H. Scanlan, E. Simiu, F. Sisto, A Modern Course in Aeroelasticity, Springer Science, USA (2006).

[7] H. Dai, X. Yue, D. Xie, S. Atluri, Chaos and chaotic transients in an aeroelastic system, Journal of Sound and Vibration 333 (2014) 7267–7285.

[8] A. Abdelkefi, R. Vasconcellos, F. Marques, M. Hajj, Modeling and identification of free play nonlinearity, Journal of Sound and Vibrations 331 (2012) 1898–1907.

[9] A. Desai, S. Sarkar, Analysis of nonlinear aeroelastic system with paramet- ric uncertainties using polynomial chaos expansion, Mathematical Problems in Engineering 21 (2010) 1–21.

[10] M. Kehoe, A Historical overview of Flight Flutter Testing, NASA TM-4270 (1985).

[11] N. Zimmerman, J. Weissenburger, Prediction of flutter onset speed based on flight testing at subcritical speeds, Journal of Aircraft 1 (1964) 190–202.

[12] S. J. Price, B. H. K. Lee, Evaluation and extension of the flutter-margin method for flight flutter prediction, Journal of Aircraft 30 (1993) 395–402.

[13] R. Lind, M. Brenner, Flutterometer : An on-line tool to predict robust flutter margins, Journal of Aircraft 37 (2000).

[14] T. Strganac, G. Platanitis, Wind Tunnel Testing of the NASA-DFRC Flutterometer using a Two DOF Wing Section, Technical report, NASA, USA, http://ntrs.nasa.gov/archive/nasa/casi.ntrs.nasa.gov/20010097722.pdf (2001).

[15] C. Popescu, Y. Wong, B. Lee, An expert system for predicting nonlinear aeroelastic behavior of an airfoil, Journal of Sound and Vibration 319 (2009) 1312–1329.

[16] M. Schwartz, S. Manzoor, P. Hemon, E. de Langre, By-pass transition to airfoil flutter by transient growth due to gust impulse, Journal of Fluids and Structures 25 (2009) 1272–1281.

[17] D. Poirel, Random Dynamics of a Structurally Nonlinear Airfoil in Turbulent flow, PhD thesis, McGill University, Montreal, Canada (2001).
[18] D. Poirel, Y. Harris, A. Benaissa, Self-sustained aeroelastic oscillations of a naca0012 airfoil at low-to-moderate reynolds numbers, Journal of Fluids and Structures 24 (2008) 700–719.
[19] S. Price, J. Keleris, Nonlinear dynamics of an airfoil forced to vibrate in dynamic stall, Journal of Sound and Vibration 194 (1996) 265–283.
[20] T. Andrianne, G. Dimitriadis, Experimental analysis of the bifurcation behavior of a bridge deck undergoing across-wind galloping, in Proceedings of the 8th International Conference on Structural Dynamics, EURODYN, Leuven Belgium. ISBN 978-90-760-1931-4.
[21] B. Korbahti, E. Kagambage, T. Andrianne, N. Razak, G. Dimitriadis, Subcritical, non-typical and period-doubling bifurcations of a delta wing in a low speed wind tunnel, Journal of Fluids and Structures 27 (2011) 408–426.
[22] J. Venkatramani, V. Nair, R. I. Sujith, S. Gupta, S. Sarkar, Precursors to flutter instability by an intermittency route: a model free approach, Journal of Fluids and Structures (2014).
[23] K. Wiesenfeld, Noisy precursors of nonlinear instabilities, Journal of Statistical Physics 38 (1985) 1071–1097.
[24] E. Surovyatkina, Prebifurcation noise amplification and noise-dependent hysteresis as indicators of bifurcations in nonlinear geophysical systems, Nonlinear processes geophysics 12 (2005) 25–29.
[25] V. Jegadeesan, R. Sujith, Experimental investigating of noise induced triggering in thermoacoustic systems, Proceedings of the Combustion Institute 34 (2013) 3175–3183.
[26] B. Mandelbrot, The fractal geometry of nature, W.H. Freeman and company, New York (1982) .
[27] U. Frisch, G. Parisi, On the singularity structure of fully developed turbulence, in R. B. . G. P. M. Gil. (Ed.) In Turbulence and Predictability in Geophysical Fluid Dynamics (1985) pp. 84–88.
[28] E. Montroll, M. Schlesinger, On 1/f noise and other distributions with long tails, Proceedings of national academic science, USA 79 (1982) 3380–3383.
[29] M. Schlesinger, Fractal time and 1/f noise in complex systems, Annals of the New York academy of sciences 504 (1987) 214–228.
[30] E. Ott, Chaos in Dynamical Systems, Cambridge University Press (1993).
[31] H. Hentschel, I. Proccacia, Fracftal nature of turbulence as manifested in turbulent diffusion, Physical Review A 27 (1983) 1266–1269.
[32] H. Daniels, Saddlepoint approximation in statistics, Annals of Mathematical Statistics 25 (1954) 631–650.
[33] H. E. Hurst, Long-term storage capacity of reservoirs, Transactions of American scoiety for civil engineers 116 (1951) 770–808.
[34] J. Bassingthwaighte, L. Liebovitch, B. West, Fractal physiology, Oxford University Press (1994) .
[35] B. West, M. Latka, M. Glaubic-Latka, D. Latka, Multifractality of cerebral blood flow, Physica A 318 (2003) 453–460.
[36] C. Peng, S. Buldyrev, S. Havlin, H. Stanley, A. Goldberger, Mosaic organization of dna nucleotides, Physical Review E 49 (1994) 1685–1689.
[37] J. Kantelhardt, E. Kosciekny-Bunde, H. Rego, S. Havlin, A. Bunde, Detecting long-

range correlations with detrended fluctuation analysis, Physica A 295 (2001) 441–454.
[38] J. Kantelhardt, S. Zschiegner, E. Kosciekny-Bunde, S. Havlin, A. Bunde, Multifractal detrended fluctuation analysis of nonstationary time series, Physica A 316 (2002) 87–114.
[39] U. Frisch, Turbulence: The legacy of a.n. kolmogorov., Cambridge University Press (1995) .
[40] K. Sreenivasan, C. Meneveau, The fractal facets of turbulence, Journal of Fluid Mechanics 173 (1986) 357–386.
[41] K. Sreenivasan, C. Meneveau, Singularities of the equations of fluid motion, Physics Review A 38 (1988) 6287–6295.
[42] K. Sreenivasan, Fractals and multifractals in fluid turbulence, Annu. Rev. Fluid Mechanics 23 (1991) 539–604.
[43] G. Litak, J. Sawicki, Cracked rotor vibrations by multifractal analysis, Euromech 498 colloquim, Kazimierz, Poland 498 (2008) 1–4.
[44] W. Du, J. Tao, Y. Li, C. Liu, Wavelet leaders multifractal features based fault diagnosis of rotating mechanism, Mechanical Systems and Signal Processing 43 (2014) 57–75.
[45] Y. Lv, J. Gao, Condition prediction of chemical complex systems based on multifractal and mahalanobis-taguchi system, International Conference on Quality, Reliability, Risk, Maintenance, and Safety Engineering (ICQR2MSE) (2011) 536–539.
[46] T. Hikihara, T. Fujinami, F. Moon, Bifurcation and multifractal dynamics of a high-tc superconducting levitation system, Physics Letters A 231 (1997) 217–223.
[47] V. Pakrashi, J. Kelly, J. Harkin, A. Farrell, Hurst exponent footprints from activities on a large structural system, Physica A 392 (2013) 1803–1817.
[48] C. Xiu, T. Wang, M. Tian, Y. Li, Y. Cheng, Short-term prediction method of wind speed series based on fractal interpolation, Chaos, Solitons and Fractals 68 (2014) 89–97.
[49] L. Sun, W. Kinsner, N. Serinken, Characterization and feature extraction of transient signals using multifractal measures, Proceedings of the 1999 IEEE Canadian Conference on Electrical and Computer Engineering Shaw Conference Center, Edmonton, Alberta, Canada (1999) 781–785.
[50] F. Gouldin, An application of fractals to modeling premixed turbulent flames, Combustion flame 68 (1987) 249–266.
[51] F. Gouldin, S. Hilton, T. Lamb, Experimental evaluation of the fractal geometry, Twenty-Second International Symp. on Combustion (1988) 541–550.
[52] F. Gouldin, K. Bray, J. Chen, Chemical closure model for fractal flamelets, Combustion flame 77 (1989) 241–259.
[53] V. Nair, R. I. Sujith, Multifractality in combustion noise: predicting an impending combustion instability, Journal of Fluid Mechanics 747 (2014) 635–655.
[54] T. O'Neil, T. Strganac, Aeroelastic response of a rigid wing supported by nonlinear springs, Journal of Aircraft 35 (1998) 616–622.
[55] B. Kerres, V. Nair, A. Cronhjort, M. Mihaescu, Analysis of the turbocharger compressor surge margin using a hurst-exponent-based criterion, SAE International Journal of Engines 125 (2016) 1–11.
[56] B. West, A. Goldberger, Physiology in fractal dimensions, American science 75 (1987) 354–365.
[57] B. Lee, S. Price, Y. Wong, Nonlinear aeroelastic analysis of airfoils: bifurcations and chaos, Progress in Aerospace Sciences 35 (1999) 205–334.
[58] C. C. Marsden, S. J. Price, Transient and limit cycle simulation of a nonlinear aeroelastic

system, Journal of Aircraft 44 (2007) 60–70.
[59] E. H. Dowell, E. E. Crawley, H. C. Curtiss Jr, D. A. Peters, R. H. Scanlan, F. Sisto, A Modern Course in Aeroelasticity, Kluwer Academic Publishers, Dordrecht (1995).
[60] W. P. Jones, Summary of formulae and notations used in two dimen- sional derivative theory, Technical report, British aeronautical research committee, report and memorandum (1958).
[61] C. Meneveau, K. Sreenivasan, The multifractal nature of turbulent energy dissipation, Journal of Fluid Mechanics 24 (1991) 429–484.
[62] a. J. C. Shinozuka, M ., Digital simulation of random processes and its applications, Journal of Sound and Vibration 25 (1972) 111–128.